Int. J. Electrochem. Sci., 14 **(2019)** 6032 – 6044, doi: 10.20964/2019.07.13

International Journal of
ELECTROCHEMICAL
SCIENCE
www.electrochemsci.org

Study of the Corrosion Resistance of a Superhydrophobic Ni-P-Al_2O_3 Composite Coating Based on Electrochemical Machining

Yin Zhang[1], *Min Kang*[1,2,*], *Hengzheng Li*[1], *Yuntong Liu*[1]

[1] College of Engineering, Nanjing Agricultural University, Nanjing, 210031, China;
[2] Guanyun Research Institute for Modern Agricultural Equipment, Nanjing Agricultural University, Guanyun, 222200, China.
[*]E-mail: kangmin@njau.edu.cn

Received: 1 March 2019 / *Accepted:* 19 April 2019 / *Published:* 10 June 2019

To enhance the corrosion resistance of type 45 steel substrates, a superhydrophobic Ni-P-Al_2O_3 composite coating was prepared on the type 45 steel substrates with electrochemical machining. The surface morphology, surface roughness, wettability and corrosion resistance of the coating were investigated by using scanning electron microscopy, laser scanning confocal microscopy, optical contact angle measurements and electrochemical analysis. The results show that an irregular micropit structure is obtained after the Ni-P-Al_2O_3 composite coating was prepared by electrochemical dissolution and fluorosilane modification. There is an obvious increase in the surface roughness of the Ni-P-Al_2O_3 composite coating. The water contact angle reaches 152.3 degrees on the coating surface. After 25 days, a high hydrophobicity remains, and the water contact angle is 153.4 degrees. Approximately 89.72% of the droplet volume is in contact with air. The superhydrophobic Ni-P-Al_2O_3 composite coating exhibits a higher corrosion potential of E_{corr}=-0.282 V and a lower corrosion current density of J_{corr}=7.018×10^{-7} A/cm^2 compared to the type 45 steel substrates. The polarization curves of the coating at different times were studied in a 5 wt% NaCl solution to investigate the stability of the superhydrophobic Ni-P-Al_2O_3 composite coating. The maximum corrosion current density of the superhydrophobic Ni-P-Al_2O_3 composite coating is 10.254×10^{-6} A/cm^2, and the corrosion rate is 0.124 mm/year. The superhydrophobic Ni-P-Al_2O_3 composite coating has excellent corrosion resistance.

Keywords: Electrochemical machining, Ni-P-Al_2O_3 composite coating, Surface roughness, Wettability, Corrosion resistance

1. INTRODUCTION

Metals and their alloys are important engineering materials. The corrosion products on metals can be concealed, which results in premature failure of metallic components, massive economic losses and environmental contamination [1]. There are different techniques for preventing the corrosion of

metals. One is the coating of a metal surface with an anticorrosive layer to provide a barrier between the metal surface and the corrosive environment [2-3].

Ni-P alloy coatings have been employed in industrial applications due to their excellent properties, such as corrosion and wear resistance. The corrosion behavior of Ni-P deposits has been studied by many scholars [4-7]. Nanocomposite coatings with better wear resistance and corrosion resistance can be obtained by adding nanoparticles into a Ni-P alloy matrix. Tamilarasan made Ni-P-rGO coatings on low carbon steel substrates by electroless plating and found that the addition of rGO particles considerably improved the corrosion [8]. Wang made Ni-P-diamond coatings by electroless plating and found that the addition of diamond particles could substantially improve the wear resistance [9]. A Ni-P-CeO_2-RuO_2 coating exhibited a higher corrosion potential of E_{corr}=-0.349 V and a lower corrosion current density of J_{corr}=12 μA/cm^2 compared to Ni-P alloys [10]. It was found that incorporation of nano-Al_2O_3 improves the corrosion resistance of a steel specimen [11]. Karthikeyan found that the specific wear rate of a Ni-P-Al_2O_3 coating was lower when compared with that of a Ni-P coating [12]. Sadreddini showed that the incorporation of Al_2O_3 in a Ni-P coating led to a low corrosion rate by electrochemical impedance spectroscopy (EIS) and polarization techniques [13]. Chen reported that a Ni-P-Al_2O_3 coating had better corrosion resistance compared to that of a Ni-P coating on mild steel [14].

Recently, superhydrophobic surfaces have gained scientific and technical interest due to their attractive properties [15], such as self-cleaning [16], anti-icing [17], anti-fogging [18] and corrosion resistance [19]. The preparation methods for superhydrophobic surfaces have advanced considerably. These include nanosecond lasers [20], laser etching [21], anodization [22], electron discharge machining [23], surface template transfer [24] and electrochemical deposition [25,26]. However, these processes have disadvantages. For example, it is difficult to prepare large areas, and they also require complex equipment. Compared with other methods for preparing superhydrophobic surfaces, electrodeposition is an effective technique for fabricating superhydrophobic coatings and includes the advantages of low cost, reproducibility, scalability, and simplicity, which permit its use for a range of applications [27-29].

In this study, we use an electrodeposition technique to prepare a Ni-P-Al_2O_3 composite coating. The coating is processed by electrochemical dissolution and fluorosilane modification. Scanning electron microscopy is employed to analyze the surface morphology. Moreover, the surface roughness, wettability and corrosion resistance of the coatings are investigated by laser scanning confocal microscopy, optical contact angle measurements and electrochemical analysis, respectively. The superhydrophobic Ni-P-Al_2O_3 composite coating is obtained by electrochemical dissolution and fluorosilane modification. The superhydrophobic coating can provide effective protection of type 45 steel substrates. This research aims to provide an important reference value for the corrosion protection of metals. The results derived from this research may be used in future industrial applications.

2. EXPERIMENTAL

2.1 Pretreatment of substrate

Type 45 steel substrates (30 mm×8 mm×7 mm) with a chemical composition of 0.42-0.50% C, 0.17-0.37% S, 0.50-0.80% Mn, 0.035% P, 0.035% S, 0.25% Ni, 0.25% Cr and 0.25% Cu were used. A

type 45 steel substrate usually requires a series of pretreatment steps to ensure a good quality deposit. The pretreatment series started by degreasing to remove oil contamination and fingerprints and was followed by acidic etching. The last step was applied to remove the oxides and deposits. The bath composition and operating conditions employed for the preparation are given in Table 1.

Table 1. The bath composition and operating conditions of the pretreatment process used in the experiment

Process	Composition ($g \cdot L^{-1}$)	Operating conditions
#1 Degreasing	25.0 NaOH+21.7 Na_2CO_3+50.0 Na_3PO_4 +2.4 NaCl	Current 1 A, Time 25 s
#2 Acidic etching	25.0 Hydrochloric acid+140.1 NaCl	Current 1 A, Time 30 s
#3 Removal of the oxides and deposits	141.2 $Na_3C_6H_5O_7 \cdot 2H_2O$+94.3 $H_3C_6H_5O_7 \cdot H_2O$+3.0 $NiCl_2 \cdot 6H_2O$	Current 1 A, Time 30 s

2.2 Preparation of Ni-P-Al_2O_3 coating

The Ni-P-Al_2O_3 layers were obtained by electrodeposition from an aqueous solution containing 200 $g \cdot L^{-1}$ $NiSO_4 \cdot 6 H_2O$, 30 $g \cdot L^{-1}$ $NiCl_2 \cdot 6 H_2O$, 30 $g \cdot L^{-1}$ H_3BO_3, 20 $g \cdot L^{-1}$ H_3PO_3, 60 $g \cdot L^{-1}$ $C_6H_8O_7$, 0.08 $g \cdot L^{-1}$ sodium dodecyl sulfate, 0.02 $g \cdot L^{-1}$ sulfourea and 4 $g \cdot L^{-1}$ Al_2O_3 with an average particle size of 30 nm. All experiments were performed at a temperature of 60 °C, current density of 5 $A \cdot dm^{-2}$ and plating time of 90 min. During deposition, the bath was stirred. The stirring speed of the mechanical agitator was set at 1500 $r \cdot min^{-1}$ to prevent nanoparticles from precipitating. A nickel electrode (200 mm×50 mm×5 mm) was used as an anode. The cathode was a type 45 steel substrate mounted parallel to the anode plane.

2.3 Electrochemical machining

The Ni-P-Al_2O_3 composite coating was processed by electrochemical dissolution. The cathode was a 304 L stainless steel (30 mm×30 mm×1 mm), and the 1 A direct current had a voltage of 12 V. The electrochemical dissolution time was 5 min and the samples were immersed in a 0.585 wt% NaCl solution.

2.4 Treated by fluorosilane solution

The fluorosilane solution comprised fluorosilane (1%) and alcohol (99%). The fluorosilane solution was stirred for 360 min using a magnetic stirring apparatus. The Ni-P-Al_2O_3 composite coating and the coating from the electrochemical dissolution were washed by ultrasonic cleaning for 5 min and

then treated with a fluorosilane solution for 60 min. The sample was dried and then put into a sealed plastic bag.

2.5 Characterization and tests

The surface morphology of the coatings was characterized using scanning electron microscopy (SEM). The surface roughness of coatings was measured by laser scanning confocal microscopy (OLS4100), which uses S_a as an evaluation parameter, and the evaluation area was 120 μm×120 μm. The contact angle was measured by optical contact angle measurements (OCA20). The volume of the water droplet was 3 μL, and the water droplet velocity was 1 μL/s. The average value of the contact angle in five different positions was obtained. The corrosion resistance of the coatings was measured by an electrochemical workstation (CS350) in which a NaCl solution of 5 wt% was used as the corrosion medium. The scanning range was from -1 V to 1.5 V, and the scan rate was 0.5 mV/s.

3. RESULTS AND DISCUSSION

3.1 SEM images and thickness of Ni-P-Al_2O_3 composite coatings

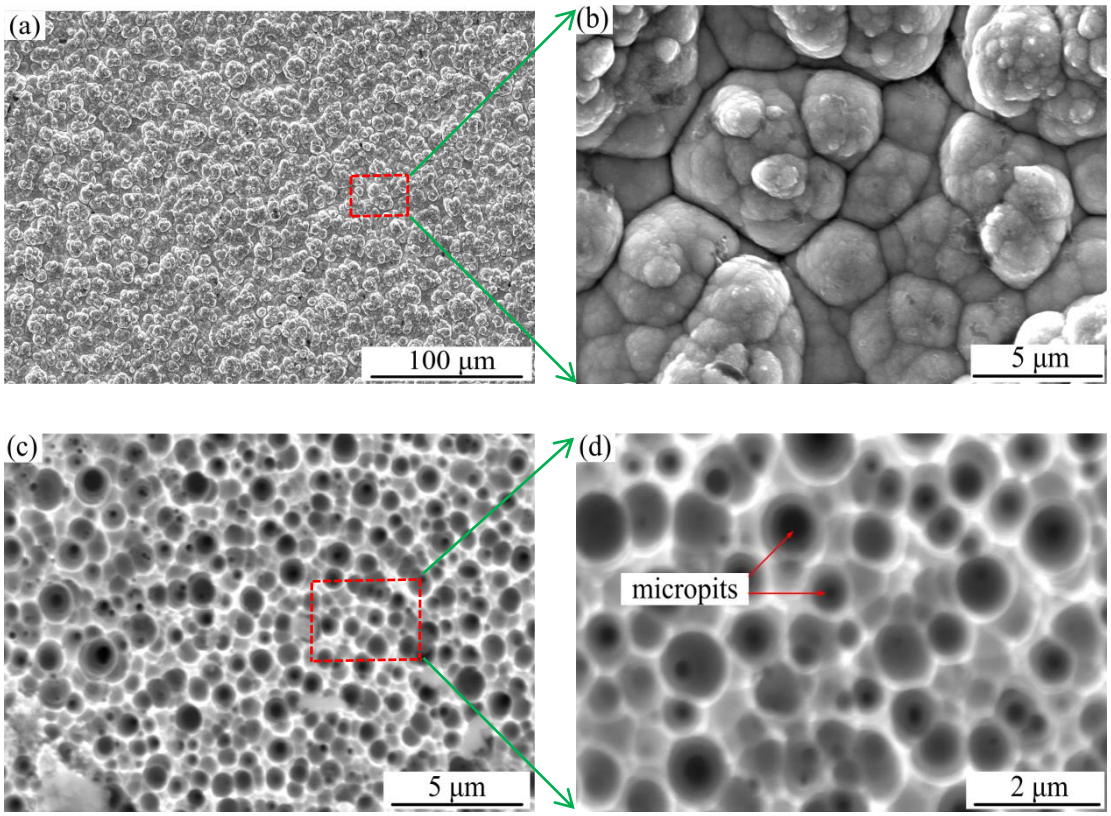

Figure 1. SEM images of coatings: (a) and (b) SEM images of the Ni-P-Al_2O_3 composite coating (5 A·dm^{-2}, 60 °C and 90 min); and (c) and (d) SEM images of the Ni-P-Al_2O_3 composite coating processed by electrochemical dissolution (1 A, 12 V and 5 min) and fluorosilane modification (60 min).

Figure 1 shows SEM images of the coatings. Figure 1a shows an SEM image of a Ni-P-Al_2O_3 composite coating prepared by electrodeposition.

Figure 1b shows a high magnification of the boxed area in Figure 1a. The surface of the Ni-P-Al_2O_3 composite coating is dense, and there are no pores. Figure 1c shows the SEM image of the Ni-P-Al_2O_3 composite coating after processing by electrochemical dissolution and fluorosilane modification. Figure 1d shows a high magnification of the boxed area in Figure 1c. The SEM image of the Ni-P-Al_2O_3 composite coating exhibits significant changes, as shown by the irregular micropit structure in Figure 1d. Figure 2 shows cross-sections of the coatings. The thickness of the Ni-P-Al_2O_3 composite coating is 34.72 μm in Figure 2a. In addition, Figure 2b shows that the Ni-P-Al_2O_3 composite coating was not completely removed after electrochemical machining.

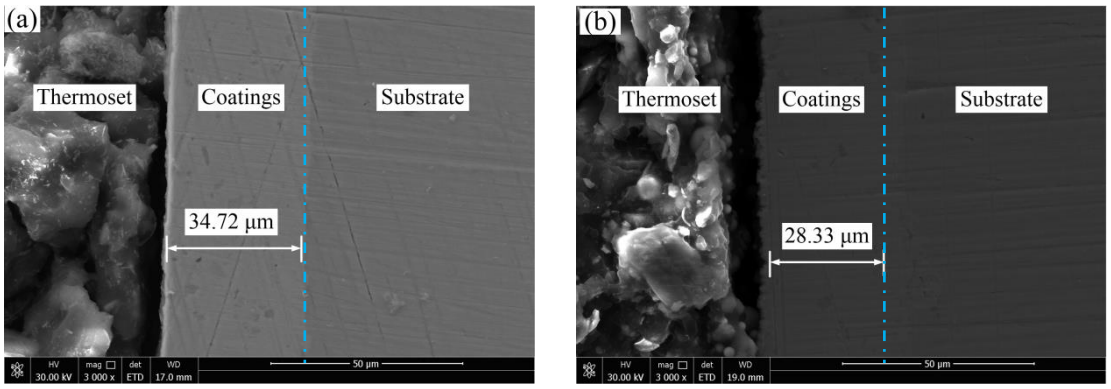

Figure 2. Cross-section of coatings: (a) cross-section of Ni-P-Al_2O_3 composite coating (5 A·dm^{-2}, 60 °C and 90 min); and (b) cross-section of the Ni-P-Al_2O_3 composite coating processed by electrochemical dissolution (1 A, 12 V and 5 min) and fluorosilane modification (60 min).

3.2 X-ray diffraction analysis of Ni-P-Al_2O_3 composite coatings

The XRD patterns of the coatings are shown in Figure 3. Figure 3a shows the XRD patterns of the Ni-P-Al_2O_3 composite coating prepared by electrodeposition. The three sharp peaks at approximately 2θ=44.706°, 52.124°, and 76.409° are assigned to be the (111), (200), and (220) diffraction peaks of Ni, respectively. Figure 3b shows the XRD patterns of the Ni-P-Al_2O_3 composite coating after processing by electrochemical dissolution and fluorosilane modification. It can be seen that the strength of the Ni peak (2θ=44.706°) clearly decreases after the electrochemical dissolution, and the two diffraction peaks that appeared at 2θ=52.124° and 2θ=76.409° prior to processing disappeared. The widening of the Ni (111) peak shows the existence of the coatings, indicating that the Ni-P-Al_2O_3 composite coating was not completely removed after electrochemical machining.

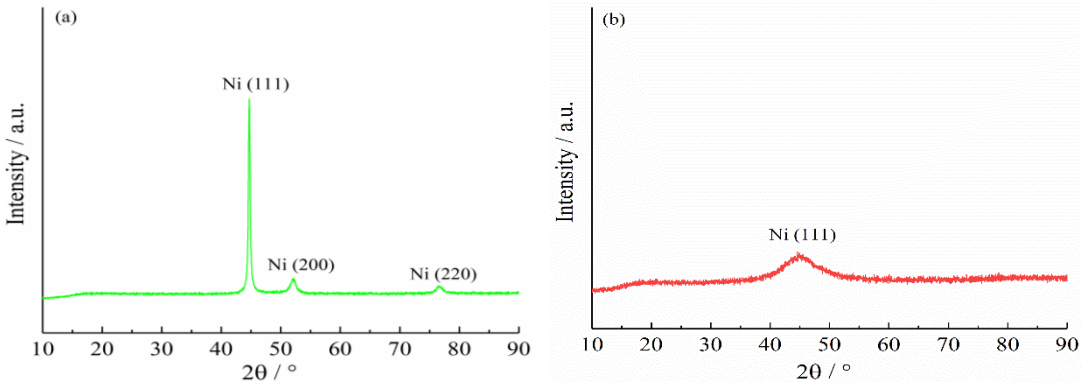

Figure 3. XRD patterns of coatings: (a) XRD pattern of the Ni-P-Al_2O_3 composite coating (5 A·dm^{-2}, 60 °C and 90 min); and (b) XRD pattern of the Ni-P-Al_2O_3 composite coating processed by electrochemical dissolution (1 A, 12 V and 5 min) and fluorosilane modification (60 min).

3.3 Surface roughness of Ni-P-Al_2O_3 composite coatings

Figure 4 shows the surface roughness S_a of the coatings. The data indicates that the surface roughness S_a of the Ni-P-Al_2O_3 composite coating is 0.52 μm (Figure 4a). Figure 4b shows the surface roughness S_a of the Ni-P-Al_2O_3 composite coating processed by electrochemical dissolution and fluorosilane modification. It can be seen that surface roughness S_a clearly increases (S_a=0.93). The surface roughness is mainly affected by the surface morphology. Wan et al. also proved that with increasing surface roughness, the spreading rate gradually decreases, and the apparent equilibrium contact angle changes from 70.2 degrees to 112.6 degrees [30]. Through observation and analysis of the surface morphology of the Ni-P-Al_2O_3 composite coating after processing by electrochemical dissolution and fluorosilane modification, it can be seen that the surface forms irregular micropits, which results in an apparent increase in the surface roughness.

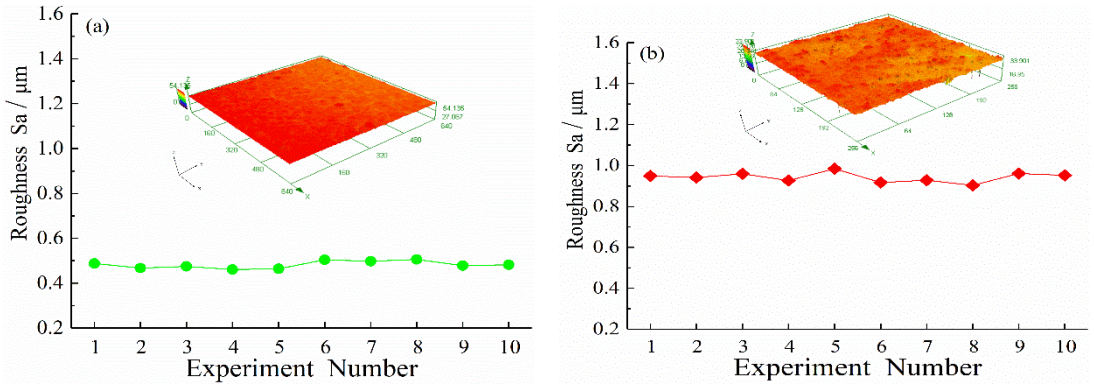

Figure 4. Surface roughness of coatings (the evaluation area, 120 μm×120 μm): (a) surface roughness of the Ni-P-Al_2O_3 composite coating (5 A·dm^{-2}, 60 °C and 90 min); and (b) surface roughness of the Ni-P-Al_2O_3 composite coating processed by electrochemical dissolution (1 A, 12 V and 5 min) and fluorosilane modification (60 min).

3.4 Wettability of Ni-P-Al_2O_3 composite coatings

Figure 5 shows the contact angle data of the coating. Figure 5a shows the contact angle data of the Ni-P-Al_2O_3 composite coating prepared by electrodeposition. The H_2O contact angle of the coating surface is approximately 88 degrees. Figure 5b shows that the contact angle of the Ni-P-Al_2O_3 composite coating processed by electrochemical dissolution and fluorosilane modification. The H_2O contact angle reaches 152.3 degrees and achieves a superhydrophobic state. A superhydrophobic surface is often created by two pathways [31]: one is the utilization of the low surface energy of hydrophobic materials, and the other is roughness creation, as in the case of lotus leaves. The SEM images in Figures 1c and 1d show an irregular micropit structure after the Ni-P-Al_2O_3 composite coating is processed by electrochemical dissolution and fluorosilane modification. As shown in Figure 4b, the surface roughness of the coatings obviously increases, and the surface energy of the coatings is lower after fluorosilane modification.

Figures 5c~5e show the contact angle images of the superhydrophobic Ni-P-Al_2O_3 composite coating after 5 days and 25 days. Although the contact angle of coatings varies slightly, the contact angle (maximum of 153.4 degrees) is still larger than 150 degrees, which indicates a high superhydrophobicity, indicating that the superhydrophobic coating has good stability. The contact angle θ is 88.3 degrees, and the Cassie-Baxter contact angle θ_{CB} is 153.4 degrees. Applying the formula $\cos\theta_{CB} = f_s \cos\theta - (1 - f_s) = f_s \cos\theta + f_s - 1$ [32,33], it was found that approximately 89.72% of the droplet volume is in contact with air, and the volume ratio between the water droplet and solid is very small. Figure 5f shows the resistance to bonding of the Ni-P-Al_2O_3 composite coating. Figures 6(a) and 6(b) show images of the Ni-P-Al_2O_3 composite coating before and after electrochemical machining.

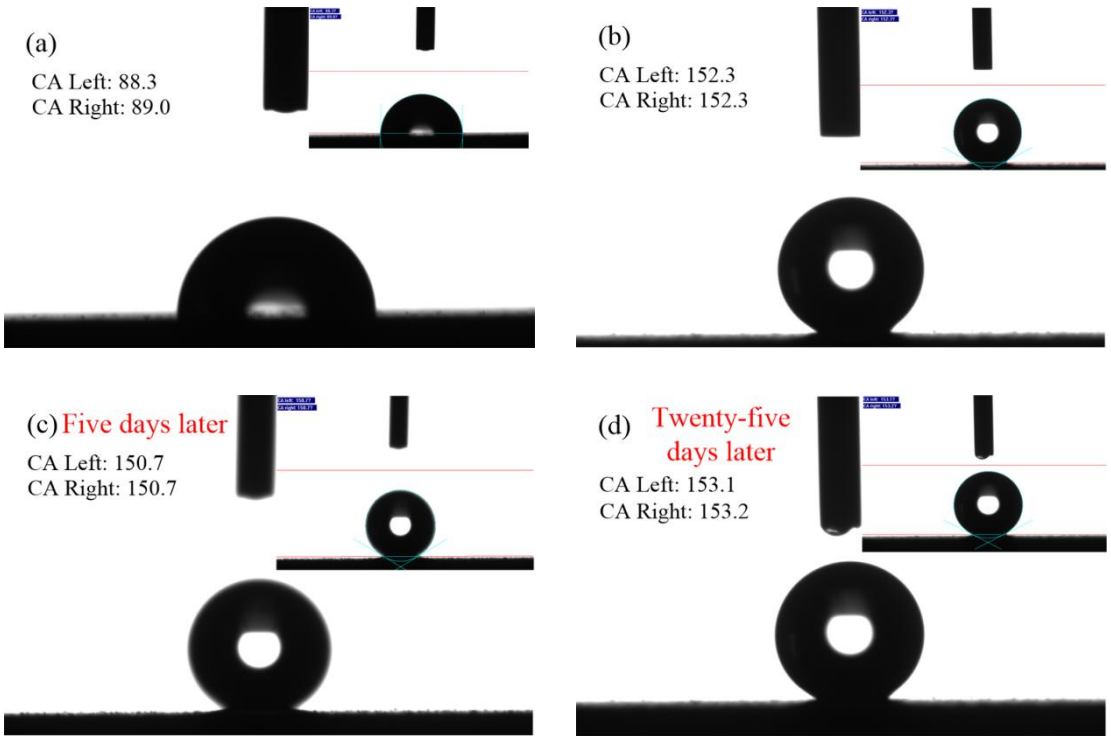

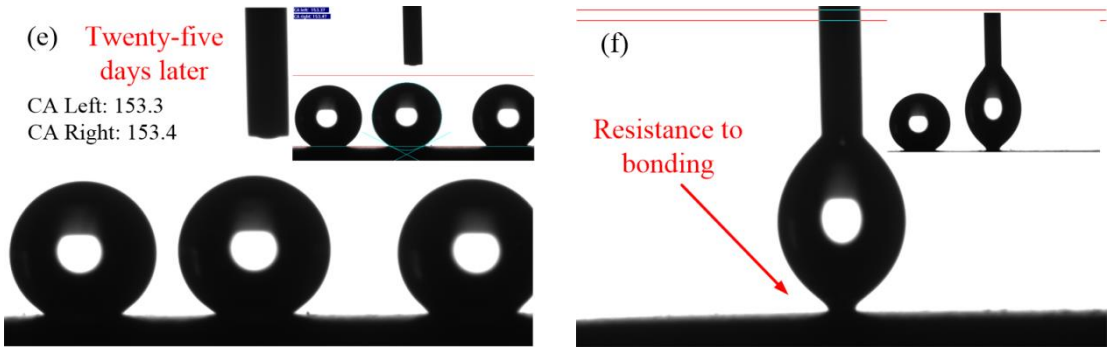

Figure 5. The contact angle of the coating surface (the volume, 3 μL; the velocity, 1 μL/s)

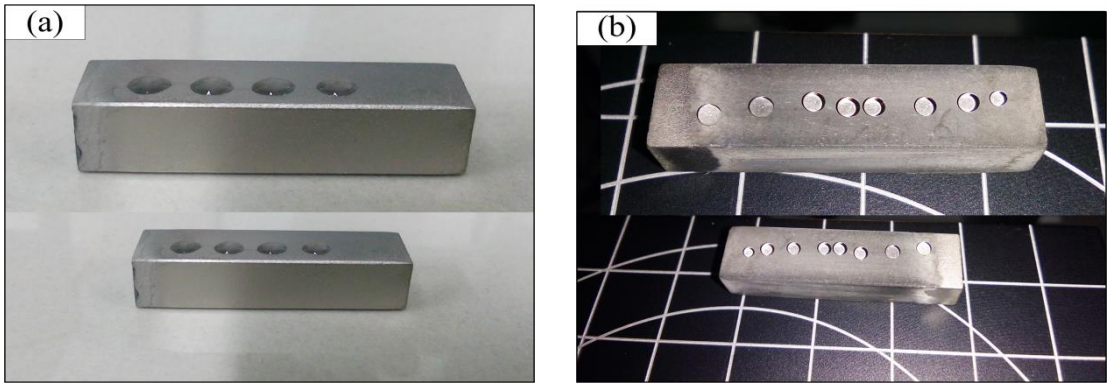

Figure 6. (a) and (b) Images of the Ni-P-Al_2O_3 composite coating before and after electrochemical machining (the volume, 3 μL; the velocity, 1 μL/s)

3.5 Corrosion resistance of Ni-P-Al_2O_3 composite coatings

Figure 7 shows the polarization curves for the type 45 steel substrate and the Ni-P-Al_2O_3 coating when immersed in a 5 wt% NaCl solution. Table 2 lists the electrochemical dynamic parameters. Dey [34] found that a strong synergy exists between the maximum corrosion resistance and maximum hydrophobicity. The higher the contact angle, the better the corrosion resistance of coating would be. When the immersion time is 0.5 h in NaCl solution, the corrosion potential of the type 45 steel substrate is -0.763 V, and the current density is 8.190×10^{-6} A/cm^2. The corrosion potential of the Ni-P-Al_2O_3 composite coating is -0.622 V, and the current density is 2.045×10^{-6} A/cm^2. The corrosion rate of the Ni-P-Al_2O_3 composite coating is 0.025 mm/year. This indicates that the Ni-P-Al_2O_3 composite coating can effectively protect type 45 steel substrates. Compared with that of the Ni-P-Al_2O_3 composite coating, the corrosion current density of the superhydrophobic Ni-P-Al_2O_3 composite coating decreases, reaching 7.018×10^{-7} A/cm^2. The corrosion rate is only 0.008 mm/year, which indicates that the superhydrophobic Ni-P-Al_2O_3 composite coating has an excellent corrosion resistance, which is consistent with a previous report by Sun [35].

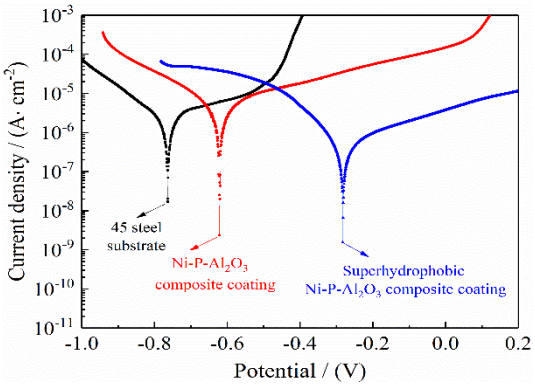

Figure 7. Potentiodynamic polarization curves of type 45 steel substrates and coatings (at 5 wt% NaCl solution; the scanning range, -1 V ~ 1.5 V; the scan rate , 0.5 mV/s)

As shown in Figures 1c and 1d, the superhydrophobic Ni-P-Al_2O_3 composite coating has an irregular micropit structure, which results in a large amount of air remaining in the superhydrophobic coating. This can form a protective "air cushion" layer on the surface of the coating. It then becomes difficult for Cl^- in the corrosion solution to get close to the substrate. Thus, the superhydrophobic Ni-P-Al_2O_3 composite coating has excellent corrosion resistance. Ou [36] showed that the Mg-H_2O-(PA/Ce)n-HDMS has much better corrosion resistance due to the retained thin layer of air at the solid/water interface in the NaCl aqueous solution. Zheng [37] reported a hierarchical superhydrophobic coating (SHPC), which shows excellent corrosion resistance with protection efficiency of 99.75%. Tang [38] mentioned the superhydrophobic surface offers a superior and stable anticorrosion protection to Al alloy in various corrosive environments. Besides, LI [39] found that the superhydrophobic coatings could supply efficient and long-term preservation for the bare Al substrate by the polarization curve and electrochemical impedance spectroscopy (EIS). In this paper, the Ni-P-Al_2O_3 composite coating with superhydrophobic surface exhibited excellent performance in terms of corrosion potential and corrosion density. The research results are similar to their conclusions.

Table 2. Fitting parameters of polarization curves of type 45 steel substrates and coatings when immersed in a 5 wt% NaCl solution

Time (h)	Different surfaces	E_{corr} (V)	J_{corr} (A/cm^2)	Corrosion rate (mm/year)
0.5	45 steel substrate	-0.763	8.190×10^{-6}	0.099
0.5	Coatings	-0.622	2.045×10^{-6}	0.025
0.5	Superhydrophobic coatings	-0.282	7.018×10^{-7}	0.008

To investigate the stability of the superhydrophobic coating in a corrosive medium, the substrates were immersed in a 5 wt% NaCl solution. Figure 8 shows that the polarization curves change with

different immersion times (0.5 h, 1 h, 6 h, 12 h, 24 h, 48 h and 72 h). The data were collected by potentiodynamic scanning. Tafel curves (traditional method) were used to fit the data, and the corrosion potential and corrosion current density were obtained. Table 3 lists the three parameters for the superhydrophobic coating obtained by fitting the polarization curves.

It is known from Figure 8 and Table 3 that the corrosion potential of the superhydrophobic coating increases from 0.5 h to 1 h, and the polarization curve moves in the positive direction, up to -0.256 V. After that, the polarization curve moves in the negative direction. With the immersion time ranging from 0.5 h to 72 h, the corrosion current density and the corrosion rate decrease first and then increase. When the immersion time is 1 h, the corrosion current density and the corrosion rate are lowest. This is because Ni^{2+} forms corrosion products, which aggregate on the surface of the electrode and hinder corrosion. The continuous formation of corrosion products on the coating surface and their barrier effect that leads to reduction of current density [40]. With prolonged immersion time, the original oxide layer on the electrode surface becomes thinner. Although the corrosion product can retard the corrosion process, the reaction of the Cl^- and metal is strong, and the corrosion rate increased. With the immersion time ranging from 0.5 h to 48 h, it can be seen that the maximum corrosion current density of the superhydrophobic coating is 8.072×10^{-6} A/cm^2, and the corrosion rate is 0.097 mm/year when the immersion time is 48 h. Although the corrosion current density and corrosion rate increase, they are still much lower than those of the type 45 steel substrates. Therefore, the superhydrophobic coating has excellent corrosion resistance and can effectively protect the type 45 steel substrates.

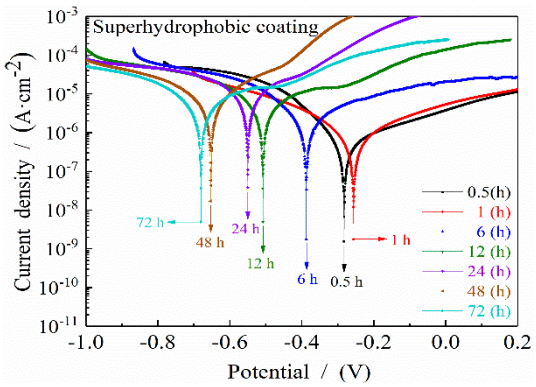

Figure 8. Potentiodynamic polarization curve of superhydrophobic Ni-P-Al_2O_3 coatings at different immersion times (at 5 wt% NaCl solution; the scanning range, -1 V~1.5 V; the scan rate, 0.5 mV/s)

In an electrochemical corrosion environment, Ni can form an oxide, which effectively hinders corrosion. The original oxide begins to dissolve first, as shown in reaction (1); then, the metal within the coating in the corrosion solution undergoes active dissolution, as shown in reaction (2). As the immersed time continues, Ni^{2+} reacts further with water to produce corrosion products, as shown in reaction (3). Namely:

$$NiO + H_2O \rightarrow Ni^{2+} + 2OH^- \quad (1)$$

$$Ni \rightarrow Ni^{2+} + 2e^{-} \quad (2)$$

$$Ni^{2+} + 2H_2O \rightarrow Ni(OH)_2 + 2H^{+} \quad (3)$$

Table 3. Fitting parameters of polarization curves of superhydrophobic coating at different times

Time (h)	E_{corr} (V)	J_{corr} (A/cm^2)	Corrosion rate (mm/year)
0.5	-0.282	7.018×10^{-7}	0.008
1	-0.256	6.254×10^{-7}	0.007
6	-0.387	3.097×10^{-6}	0.037
12	-0.507	6.606×10^{-6}	0.079
24	-0.549	6.755×10^{-6}	0.082
48	-0.653	8.072×10^{-6}	0.097
72	-0.706	10.254×10^{-6}	0.124

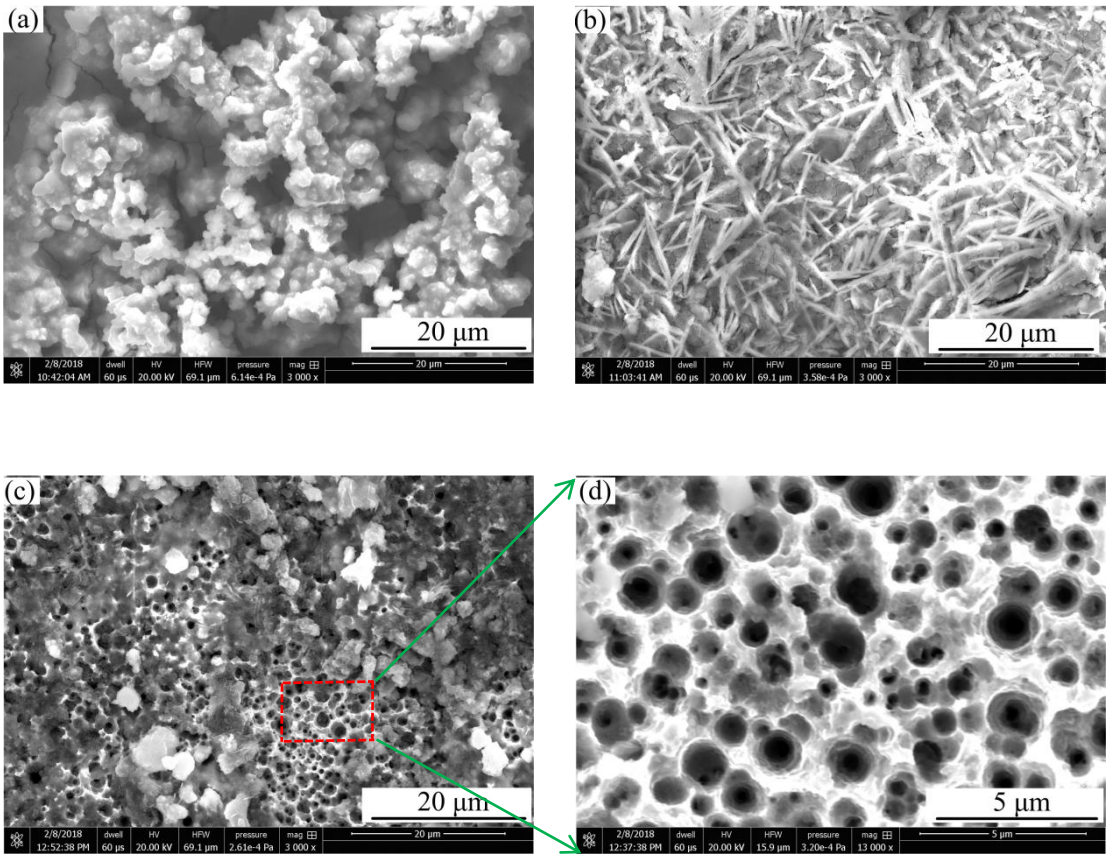

Figure 9. Images of the corrosion on the type 45 steel substrate and coatings (at 5 wt% NaCl solution): (a) corrosion image of the type 45 steel substrate; (b) corrosion image of the Ni-P-Al_2O_3 composite coating; and (c) and (d) corrosion image of the Ni-P-Al_2O_3 composite coating processed by electrochemical dissolution and fluorosilane modification (superhydrophobic Ni-P-Al_2O_3 composite coating).

Figure 9a shows an image of the type 45-steel substrate. The surface has a crack, and the corrosion products are gathered on the surface. Figure 9b shows an image of the corrosion on the Ni-P-Al_2O_3 composite coating. The corrosion products are formed and gathered on the coating surfaces. However, the corrosion morphology of the coating is completely different from that of the type 45 steel substrate. Figures 9c and 9d show an image of the corrosion on the superhydrophobic Ni-P-Al_2O_3 coating. Figure 10d shows a higher magnification of the boxed area in Figure 9c. The superhydrophobic Ni-P-Al_2O_3 coating surface also has corrosion products and is therefore still porous. This indicates that the superhydrophobic coating has excellent corrosion resistance and can play a protective role for type 45-steel substrates.

4. CONCLUSION

We successfully prepared superhydrophobic Ni-P-Al_2O_3 composite coatings by electrochemical dissolution and fluorosilane modification. The results show that an irregular micropit structure is obtained after the Ni-P-Al_2O_3 composite coating is processed by electrochemical dissolution and fluorosilane modification. The surface roughness of the Ni-P-Al_2O_3 composite coating clearly increases. The water contact angle reaches 152.3 degrees on the coating surfaces. After 25 days, a high hydrophobicity remains, and the contact angle reaches 153.4 degrees. Approximately 89.32% of the droplet volume is in contact with the air. The superhydrophobic Ni-P-Al_2O_3 composite coating exhibits a high corrosion potential of E_{corr}=-0.282 V and a low corrosion current density of $J_{corr}=7.018\times10^{-7}$ A/cm^2 compared to the type 45 steel substrate. To investigate the stability of the superhydrophobic Ni-P-Al_2O_3 composite coating, the polarization curves and electrochemical impedance spectroscopy of the coating at different times were studied in a 5 wt% NaCl solution. The maximum corrosion current density of the superhydrophobic Ni-P-Al_2O_3 composite coating is 10.254×10^{-6} A/cm^2, and the corrosion rate is 0.124 mm/year. The superhydrophobic Ni-P-Al_2O_3 composite coating has excellent corrosion resistance and plays a protective role for type 45-steel substrates.

ACKNOWLEDGEMENTS
The authors would like to acknowledge the Research and Innovation Program for Graduate Students in Jiangsu,Grant No. KYCX17_0646 and the technology development programme for the Northern Jiangsu area, Grant No. BN2014019.

CONFLICTS OF INTEREST
The authors declare no conflicts of interest.

References

1. L. Ejenstam, L. Ovaskainen, I. Rodriguez-Meizoso, L. Wågberg, J.S. Pan, A.Swerin and P.M. Clasesson, *J. Colloid Interface Sci.*, 412 (2013) 56.
2. G. Momen and M. Farzaneh, *Appl. Surf. Sci.*, 299 (2014) 41.
3. P. Wang, D. Zhang and Z. Lu, *Corros. Sci.*, 90 (2015) 23.
4. H.B. Lee, D.S. Wuu, C.Y. Lee and C.S. Lin, *Tribol. Int.*, 43 (2010) 235.
5. S.X. Jiang and R.H. Guo, *Surf. Coat. Technol.*, 205 (2011) 4274.

6. H.B. Lee, D.S. Wuu, C.Y. Lee, C.S. Lin and C.S. Lin, *Tribol. Int.*, 44 (2011) 1603.
7. Y. Liu, D. Beckett and D. Hawthorne, *Appl. Surf. Sci.*, 257 (2011) 4486.
8. T.R. Tamilarasan, U. Sanjith, M.S. Shankar and G. Rajagopal, *Wear.*, 390 (2017) 385.
9. J. Wang, F.L. Zhang, T. Zhang, W.G. Liu, W.X. Li and Y.M. Zhou, *Int. J. Refract. Met. Hard Mater.*, 70 (2017) 32.
10. S.M.A. Shibli, A.H. Riyas, M.A. Sha and R. Mole, *J. Alloys Compd.*, 696 (2017) 595.
11. M.I. Ansari, S. Julka and D.G. Thakur, *J. Mol. Liq.*, 247 (2017) 22.
12. S. Karthikeyan and B. Ramamoorthy, *Appl. Surf. Sci.*, 307 (2014) 654.
13. S. Sadreddini, S.R. Ardakani and H. Rassaee, *J. Mater Eng Perform.*, 26 (2017) 2032.
14. Y. Chen, Y.L. Hao, W. Huang, Y. Ji, W.Z. Yang, X.S. Yin, Y. Liu and X. Ling, *Surf. Coat. Technol.*, 310 (2017) 122.
15. S.F. Wang, J.L. Sha, W. Wang, C.R. Qin, W. Li and C.Q. Qin, *Carbohydr. Polym.*, 195 (2018) 39.
16. S. Nishimoto, B. Bhushan, W. Li, A. Amirfazli and W. Barthlott, *RSC Adv.*, 3 (2012) 671.
17. P. Guo, Y. Zheng, M. Wen , M.G. Wen, C. Song, Y.C. Lin and L.Jiang, *Adv. Mater.*, 24 (2012) 2642.
18. P.S. Brown, O.D. Atkinson and J.P. Badyal, *ACS Appl. Mater. Interfaces*, 6 (2014) 7504.
19. D.M. Zang, R.W. Zhu, C.X. Wu, X.Q. Yu and Y.F. Zhang, *Scr. Mater.*, 69 (2013) 614.
20. L.Y. Hu, L. Zhang, D.R. Wang, X.C. Lin and Y.Q. Chen, *Colloid Surf., A,* 555(2018)515.
21. J.H. Kim, A. Mirzaei, H.W. Kim and S.S. Kim, *Appl. Surf. Sci.*, 439 (2018) 598.
22. S.Y. Li, X.G. Xiang, B.H. Ma and X.D. Meng, *J. Alloys Compd.*, 779(2019)219.
23. S.L. Dong, Z.L. Wang, Y.K. Wang, X.L. Bai, Y.Q. Fu, B. Guo, C.L. Tan, J. Zhang and P.A. Hu, *ACS Appl. Mater. Interfaces*,10(2018)2174.
24. F.N. Viechineski, E.T. Kubaski, S. Schmidt, T. Sequinel, J.A. Varela and S.M. Tebcherani, *Surf. Eng.*, 34(2018)121.
25. C.L. Chen, Y. Fan, Y. He, X. Chen and Q.B. Yang, *Surf. Innov.*, 6(2018)106.
26. A. Fihri, D. Abdullatif, H.B. Saad, R. Mahfouz, H. Al-Baidary and M. Bouhrara, *Prog. Org. Coat.*,127(2019)110.
27. F. Su and K. Yao, *ACS Appl. Mater. Interfaces*, 6 (2014) 8762.
28. Y. Liu, S. Li, J. Zhang, J. Liu, Z. Han and L. Ren, *Corros. Sci.*, 94 (2015) 190.
29. F. Su, K. Yao, C. Liu and P. Huang, *J. Electrochem Soc.*, 160 (2013) D593.
30. B. Wan, H.R. Zhang, M. Gao, P. Bai and H. Zhang, *Mater. Design.*, 138 (2017) 103.
31. C. Anitha, S.S. Azim and S. Mayavan, *Appl. Surf. Sci.*, 449 (2017) 250.
32. Y.Y. Yan, N. Gao and W. Barthlott, *Adv. Colloid Interface Sci.*, 169 (2011) 80.
33. A.B.D. Cassie, *Discuss Faraday Soc.*, 3 (1948) 11.
34. S. Dey, S. Chatterjee, B.P. Singh, S. Bhattacharjee, T.K. Rout, D.K. Sengupta and L. Besra, *Surf. Coat. Technol.*,341(2018)24.
35. Y.K. Sun, D.Y. Zhao, J.L. Song, C. Wang, Z.H. Zhang, L. Huang and Z.A. Liu, *Res. Phys.*, 12(2019)1082.
36. J. Ou and X. Chen, *J. Alloys Compd.*, 787 (2018) 145.
37. S. Zheng, C. Li, Q. Fu, W. Hu, T. Xiang, Q. Wang, M. Du, X. Liu and Z. Chen, *Mater. Design.*, 93 (2016) 261.
38. M.K. Tang, X.J. Huang, X.W. Li, Z.Y. Huang, S.M. Zhang and Q.X. Zhang, *Mater. Express.*, 6 (2016) 101.
39. J. Li, R. Wu, Z. Jing, L. Yan, F. Zha and Z. Lei, *Langmuir.*, 31 (2015) 10702.
40. M. Golabadi, M. Aliofkhazraei, M. Toorani and A. Sabour Rouhaghdam, *J. Ind. Eng. Chem.*,47 (2017) 154.